Journal of the Taiwan Institute of Chemical Engineers 172 (2025) 106115

Contents lists available at ScienceDirect

Journal of the Taiwan Institute of Chemical Engineers

journal homepage: www.journals.elsevier.com/journal-of-the-taiwan-institute-of-chemical-engineers

Tannic acid/doxorubicin hybrid nano-assemblies decorated with D-α-tocopheryl polyethylene glycol succinate-conjugated pemetrexed to treat non-small cell lung cancer

Wei-Jen Huang [a,1], Wen-Hsuan Chiang [a,1], Hsiang-Yun Chih [a], I-Ju Liu [a], Jeng-Sen Tseng [b,c,d,e,f,*], Tsung-Ying Yang [b,f,g,h]

[a] Department of Chemical Engineering, i-Center for Advanced Science and Technology (iCAST), National Chung Hsing University, Taichung 402, Taiwan
[b] Department of Chest Medicine, Taichung Veterans General Hospital, Taichung 407, Taiwan
[c] Department of Post-Baccalaureate Medicine, College of Medicine, National Chung Hsing University, Taichung 402, Taiwan
[d] School of Medicine, National Yang Ming Chiao Tung University, Taipei 112, Taiwan
[e] Institute of Biomedical Sciences, National Chung Hsing University, Taichung 402, Taiwan
[f] Lung Cancer Comprehensive Care and Research Center, Taichung Veterans General Hospital, Taichung 407, Taiwan
[g] Rong Hsing Translational Medicine Research Center, National Chung Hsing University 402, Taichung, Taiwan
[h] Program in Translational Medicine, National Chung Hsing University 402, Taichung, Taiwan

ARTICLE INFO

Keywords:
Non-small cell lung cancer
Intracellular DOX delivery
Pemetrexed
Nano-assemblies
Folate receptor targeting

ABSTRACT

Background: The resistance of non-small cell lung cancer (NSCLC) to certain chemotherapy reagents is one of the hurdles to potent lung cancer treatment.
Methods: To amplify the cytotoxicity of doxorubicin (DOX), a frequently utilized chemotherapy drug, against NSCLC, the DOX-encapsulated hybrid nano-assemblies with folate receptor-targeting ability were fabricated using a one-step and organic solvent-free method. The amphiphilic D-α-tocopheryl polyethylene glycol succinate (TPGS) was conjugated with pemetrexed (PEM, folate analog) by esterification. Through the electrostatic and π-π stacking interactions between tannic acid (TA) and DOX, the TA/DOX nano-assemblies were attained and then coated with TPGS-PEM conjugates to obtain TA/DOX@TPGS-PEM nano-assemblies (TDTPNs).
Significant findings: The TDTPNs exhibited a high DOX payload (15.4 wt %) and a well-dispersed spherical shape. Also, the TDTPNs displayed satisfied colloidal stability in the serum-rich milieu and prevented premature DOX leakage. Through folate receptor-mediated endocytosis, the TDTPNs were efficiently internalized by LL/2 cells. Compared to free DOX molecules, the TDTPNs promoted intracellular DOX accumulation upon TPGS-mediated P-glycoprotein inactivation, thus effectively killing LL/2 cells. Furthermore, the TDTPNs exhibited cytotoxicity on LL/2 and PC9 cells superior to TA/DOX@TPGS nano-assemblies (without PEM decoration). These findings indicate that the TDTPNs showed promising potential for enhancing DOX chemotherapy against NSCLC.

1. Introduction

Lung cancer, divided into non-small cell lung cancer (NSCLC) and small cell lung cancer (SCLC), is the second-most frequently diagnosed cancer in both men and women and often leads to high mortality due to tumor metastasis [1–3]. The most frequent subtype is NSCLC (90 %) [2,3]. Unfortunately, when lung cancer patients are diagnosed, over 70 % of them have emerged with locally advanced or metastatic disease, and below 16 % have a 5-year survival rate [4]. Currently, various therapeutic modalities utilized for lung cancer treatment include surgery, chemotherapy, and/or radiation therapy [5]. As reported in several clinical cases, due to rapid attack of pulmonary metastases through the lungs, tumor elimination is quite tough [6]. Consequently, to prolong the survival of patients in the last stages of lung cancer, systemic chemotherapy is the preferred strategy of treatment [7,8]. Though in the last stages, in addition to cisplatin and carboplatin frequently employed in the first-line chemotherapy, other chemotherapy reagents (paclitaxel, irinotecan, gemcitabine, and doxorubicin

* Corresponding author.
E-mail address: tzeng64@gmail.com (J.-S. Tseng).
[1] These authors contributed equally to this work.

https://doi.org/10.1016/j.jtice.2025.106115
Received 21 December 2024; Received in revised form 22 March 2025; Accepted 24 March 2025

(DOX)) are often used. Among them, DOX is the most effective [4,9]. Furthermore, DOX is one of the most widely used and effective chemotherapy agents for the treatment of various cancers, including breast cancer, hepatoma, leukemia, lymphoma, and sarcomas [10–12]. However, the clinical application of systemic DOX chemotherapy was largely restricted due to its adverse effects on normal cells and multidrug resistance of cancer cells [9,13,14].

To reduce undesired drug side effects and promote drug accumulation in tumors, various nanoparticles such as liposomes, polymeric micelles, nano-assemblies, nanogels, and metal-organic frameworks have been widely utilized as chemotherapy drug vehicles [2–4,15–20]. Because solid tumors exhibit the inherent enhanced permeability and retention (EPR) effect, these therapeutic nanoparticles were passively deposited within tumor sites to increase drug concentration and reduce off-target-based adverse effects. For example, Melguizo et al. developed biodegradable poly(butylcyanoacrylate) (PBCA) nanoparticles as DOX carriers [4]. DOX-carrying PBCA nanoparticles remarkably increased cellular internalization of DOX by the A549 and LL/2 lung cancer cell lines, thus boosting the anticancer potency. Moreover, to achieve targeted delivery of DOX into lung tumors, Moradi et al. created SP5–52 peptide-conjugated exosome nanoparticles [2]. Compared to free DOX molecules and non-targeted DOX-loaded exosomes, the SP5–52 peptide-conjugated DOX-loaded exosomes exhibited promoted cellular uptake and cytotoxicity on LL/2 lung cancer, thus effectively inhibiting LL/2 tumor growth. As reported by Moles and co-workers [20], through the complexing of PEGylated liposomal DOX (Caelyx) with polyethylene glycol (PEG)/epidermal growth factor receptor (EGFR) bispecific antibody fragment, the EGFR-targeting DOX-loaded liposomes were attained and prominently targeting EGFR-overexpressed NSCLC to suppress H460 tumor growth in vivo. To achieve the synergistic inhibition of NSCLC, Zhou's group developed synergistic nanoparticles composed of cationic amphipathic starch and hyaluronic acid loaded with both EGFR inhibitor and DOX [3]. Although the development of nanoparticle-based DOX-carrying systems for NSCLC treatment has made considerable progress [1,3,4,13,20], the preparation of most of these nanovehicles involved the utilization of organic solvents, complicated fabrication and purification approaches, and non-degradable materials, being not preferred for practical clinical translation.

Some studies pointed out that the drug resistance of lung cancer (NSCLC and SCLC) largely decreases the efficacy of lung cancer chemotherapy [21,22]. To address this issue, the amphiphilic D-α-tocopheryl polyethylene glycol succinate (TPGS) was incorporated into various nanoparticle-based drug delivery systems. TPGS, composed of both hydrophilic (PEG chain) and hydrophobic (vitamin E) parts, has been extensively used as a surfactant, solubilizing agent, and permeation enhancer for hydrophobic drugs [23–25]. Also, TPGS potently suppresses P-glycoprotein (P-gp) meditated drug resistance in cancer cells by inhibiting P-gp activity [23–25]. As a hydrophilic small molecule with molecular structures similar to methotrexate, pemetrexed (PEM) is a multitargeted antifolate drug approved by the FDA to treat malignant pleural NSCLC and mesothelioma in 2004 [26,27]. However, the drug runs into toxicity issues at higher doses [28]. Some studies show that PEM-decorated nanoparticles could selectively recognize tumor cells from other normal cells by targeting folate receptors that are overexpressed on the cell membrane of some tumors [27,29,30].

In this work, inspired by the above studies, we fabricated the folate receptor-targeting and DOX-encapsulated nano-assemblies that promoted intracellular DOX accumulation and reduced drug resistance by one-pot method for the enhanced anticancer effect of DOX on NSCLC. First, TPGS-conjugated PEM (TPGS-PEM) conjugates were synthesized by the esterification reaction of TPGS and PEM and characterized by proton nuclear magnetic resonance (^{1}H NMR) and thermogravimetric analysis (TGA). With an organic solvent-free process, the hybrid tannic acid (TA)/DOX assemblies were fabricated upon π-π stacking and electrostatic attraction between TA and DOX molecules, followed by coating with amphiphilic TPGS-PEM conjugates through hydrophobic vitamin E anchoring combined with π-π stacking interaction to attain the TA/DOX@TPGS-PEM nano-assemblies (TDTPNs) (Scheme 1a). Herein, it should be highlighted that rare studies on combining DOX with PEM into one nano-assembly for NSCLC treatment. Furthermore, the TA/DOX@TPGS nano-assemblies (TDTNs) were prepared for comparison. The feeding weight ratios of TA/DOX assemblies to TPGS segments were optimized to increase the colloidal stability and DOX loading capability. The structural characteristics of TDTPNs were investigated by angle-dependent dynamic/static light scattering (DLS/SLS), transmission electron microscopy (TEM), and fluorescence measurements. Also, the colloidal stability and the in vitro DOX release performance of TDTPNs were assessed. The in vitro internalization of TDTPNs by LL/2 Lewis lung carcinoma cells was observed by fluorescence images. The in vitro cytotoxicity of TDTPNs on LL/2 and PC-9 cells was further evaluated.

2. Experimental section

2.1. Materials

DOX (in the hydrochloride salt form) was purchased from Carbosynth Ltd. (UK). PEM, TPGS, Dulbecco's Modified Eagle's Medium-high glucose (DMEM), 3-(4,5-Dimethylthiazol-2-yl)-2,5-diphenyltetrazolium bromide (MTT) and DMSO-d_6 were attained from Sigma-Aldrich (USA). N-(3-Dimethylaminopropyl)-N'-ethylcarbodiimide hydrochloride (EDC, 95 %) was purchased from Matrix Scientific (USA). TA (95 %) was attained from Acros Organics. Hoechst 33,342 was obtained from Invitrogen. All other chemicals were reagent grade and utilized as received. LL/2 cells (murine NSCLC line) and PC9 cells (human NSCLC line) were used in vitro experiments.

2.2. Synthesis and characterization of TPGS-PEM conjugates

According to the approach reported by Hou's group [30], the TPGS-PEM conjugates were synthesized by the esterification reaction of TPGS and PEM (Fig. 1a). In brief, EDC (18 mg) was added to DMSO (0.4 mL) containing PEM (33.4 mg). The solution was mildly stirred at 30 °C for 2 h to activate carboxyl groups of PEM molecules. Next, DMAP (11.6 mg) and TPGS (58.8 mg) in DMSO (1.2 mL) were added to the above solution and stirred for another 48 h. To remove the EDC and unreacted PEM, the solution was dialyzed (Biomate MWCO = 1 KDa) at 4 °C with deionized water. The product was then collected by lyophilization. The TPGS-PEM conjugates were characterized by ^{1}H NMR (Agilent DD2 600 MHz NMR spectrometer) using DMSO-d_6 as the solvent, UV/Vis spectrophotometer (V730, JASCO, Japan) and TGA (EXSTAR TG/DTA 6200) (Seiko Instruments Inc) in N_2 atmosphere by heating the sample to 900 °C at the rate of 10 °C/min.

2.3. Preparation of TDTNs and TDTPNs

This work fabricated TDTNs and TDTPNs using an organic solvent-free process. First, DOX (0.8 mg) and TA (1.2 mg) were separately dissolved in deionized water. Subsequently, the DOX solution was added to the TA solution and stirred at room temperature for 1 h in the dark surroundings. The resulting solution was dropwise added to the deionized water containing 2.0 mg TPGS-PEM. Afterward, the mixed solution was stirred for 24 h to obtain TDTPNs, followed by dialysis (Biomate MWCO = 12–14 KDa) with pH 8.0 phosphate buffer to eliminate the unloaded DOX, TA and TPGS-PEM. TDTNs with different feeding weight ratios of TA/DOX and TPGS and the TPGS/DOX assemblies with a weight ratio of 0.4:1 for TPGS and DOX were prepared using a similar protocol for comparison.

2.4. Physicochemical characterization

The mean hydrodynamic diameter (D_h) and polydispersity index

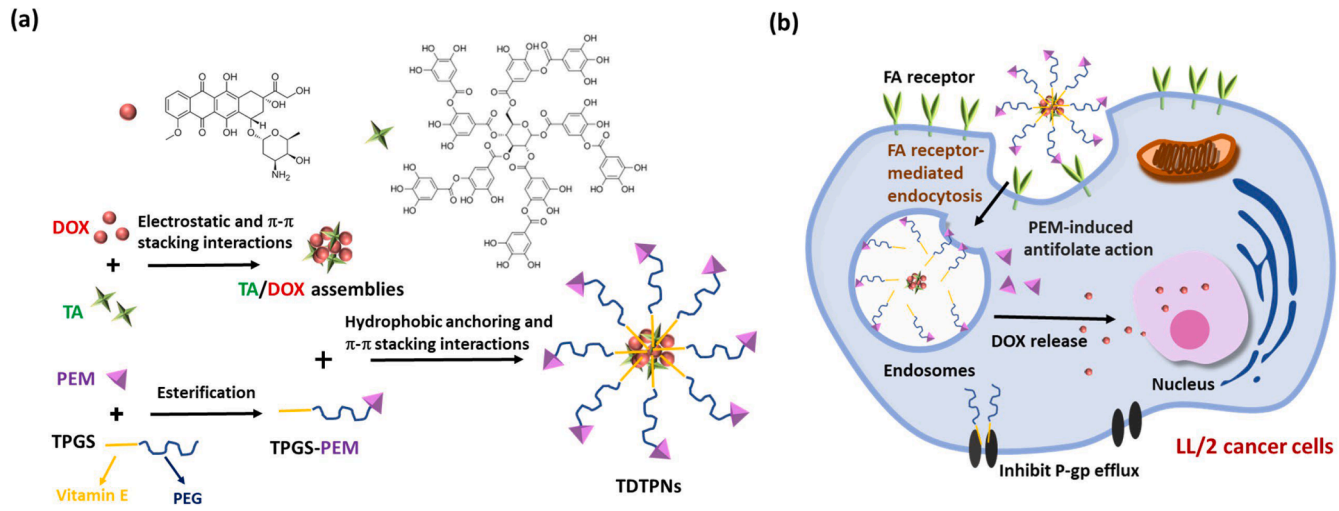

Scheme 1. Schematic presentation of (a) co-assembly between TA/DOX assemblies and TPGS-PEM conjugates to form TDTPNs and (b) intracellular DOX delivery of TDTPNs via folate receptor-mediated endocytosis.

(PDI) of TDTPNs and TDTNs in aqueous solutions were determined by DLS/SLS measurements with Brookhaven BI-200SM goniometer. Moreover, based on the measurements of the light scattering intensity at different angles using the above apparatus, the root-mean-square radius of gyration (R_g) of TDTPNs and TDTNs was obtained by the Berry plot of the scattering intensity ($I_{ex}^{1/2}$) versus the square of the scattering vector (q^2). The zeta potential value of TDTPNs and TDTNs dispersed in aqueous solutions was determined with a Litesizer 500 (Anton Paar, USA). After the triplicate measurements, the particle size and zeta potential data were averaged and presented herein. The fluorescence spectra of TDTPNs and TDTNs in aqueous solution of pH 7.4 were gained with a fluorescence spectrometer (Hitachi F-2700, Japan). The morphology of TDTPNs and TDTNs was observed by TEM (HT7700, Hitachi, Japan).

2.5. DOX loading capacity

To quantify the amount of DOX laden within TDTPNs and TDTNs, 50 μL of the purified nanoparticle solutions was freeze-dried, followed by dissolution in 1.0 mL DMSO and sonication of 1 min to disintegrate nano-assemblies. The DOX fluorescence of the resulting solution at 500–700 nm was determined with a fluorescence spectrophotometer (Hitachi F-2700) following the excitation at 480 nm. The loading efficiency (LE) and loading content (LC) of DOX were calculated as follows:

$$LE\ (\%) = \frac{weight\ of\ laden\ DOX}{weight\ of\ DOX\ in\ feed} \times 100\ \%$$

$$LC\ (wt\ \%) = \frac{weight\ of\ laden\ DOX}{weight\ of\ the\ DOX-containing\ nano-assemblies} \times 100\ \%$$

2.6. In vitro DOX liberation performance

To evaluate the DOX release from TDTPNs and TDTNs, the solutions (1.0 mL) containing these nanoparticles were placed in a dialysis tube (Biomate MWCO = 12–14 KDa), followed by dialysis against pH 7.4 phosphate buffer saline (PBS) and pH 5.0 acetate buffer (20 mL), respectively, at 37 °C. At the prescribed time intervals, the dialysate (1.0 mL) was withdrawn and replaced with the same amount of fresh medium. The DOX concentration of the dialysate was attained using the fluorescence spectrophotometer described above to determine the amount of DOX liberated from TDTPNs or TDTNs.

2.7. In vitro cellular uptake

LL/2 cells (1.5×10^5 cells/well) were dispersed in 6-well plates containing 22 mm round glass coverslips and separately treated with free DOX molecules, TDTNs, or TDTPNs at 37 °C for 1 and 4 h. DOX concentration was fixed at 10 μM. Next, the treated cells were rinsed with PBS and immobilized with 4 % formaldehyde. Hoechst 33,342 was used to stain the cell nucleus. Under a Hoechst set (Ex. 405 nm) and a DOX set (Ex. 488 nm), the cellular images of the treated LL/2 cells were observed by a confocal laser scanning microscope (CLSM, Olympus, FluoView FV3000, Japan). On the other hand, free DOX molecules, TDTNs, and TDTPNs were dispersed in DMEM to reach a DOX concentration of 10 μM. LL/2 cells were seeded in 6-well culture plates to reach a density of 1.5×10^5 cells/well and incubated with the above formulations at 37 °C for different time intervals. Subsequently, the treated cells were rinsed twice with PBS, followed by detachment with trypsin-EDTA. The cell pellet was collected by centrifugation, followed by DMSO addition for lysing cells and disrupting nanoparticles for DOX release. The fluorescence intensity of DOX (Ex. 480 nm and Em. 555 nm) was measured using a Hitachi F-2700 fluorescence spectrometer.

2.8. In vitro cytotoxicity examination

MTT assay was utilized to assess cell viability. LL/2 cells were seeded in a 96-well plate to reach 5×10^3 cells/well and incubated with DMEM at 37 °C for 24 h. After removing the culture medium, 100 μL of fresh DMEM containing free DOX molecules, TDTNs, TDTPNs at varying DOX concentrations, TPGS or TA of various concentrations was added into each well, and the cells were incubated for additional 24 h. Then, the 50 μL of MTT solution (0.5 mg/mL) was added into each well and incubated at 37 °C for 3 h. After eliminating the culture medium, the precipitate was dissolved by DMSO, and the absorbance at 570 nm was measured (BioTek 800TS microplate reader). Besides, the viability of PC9 cells (1×10^4 cells/well) treated with TDTNs and TDTPNs for 48 h was evaluated using a similar approach. For comparison, WS1 cells, human skin fibroblast cells, were incubated with TDTPNs at 37 °C for 24 h and the cell viability was assessed by MTT assay.

2.9. Statistical analysis

All experimental Data were shown as mean ± standard deviation (SD). The significance between the data in each group was calculated using ANOVA analysis: ns > 0.05, $^*p < 0.05$, $^{**}p < 0.01$, $^{***}p < 0.001$. All statistical analyses were performed using Prism software.

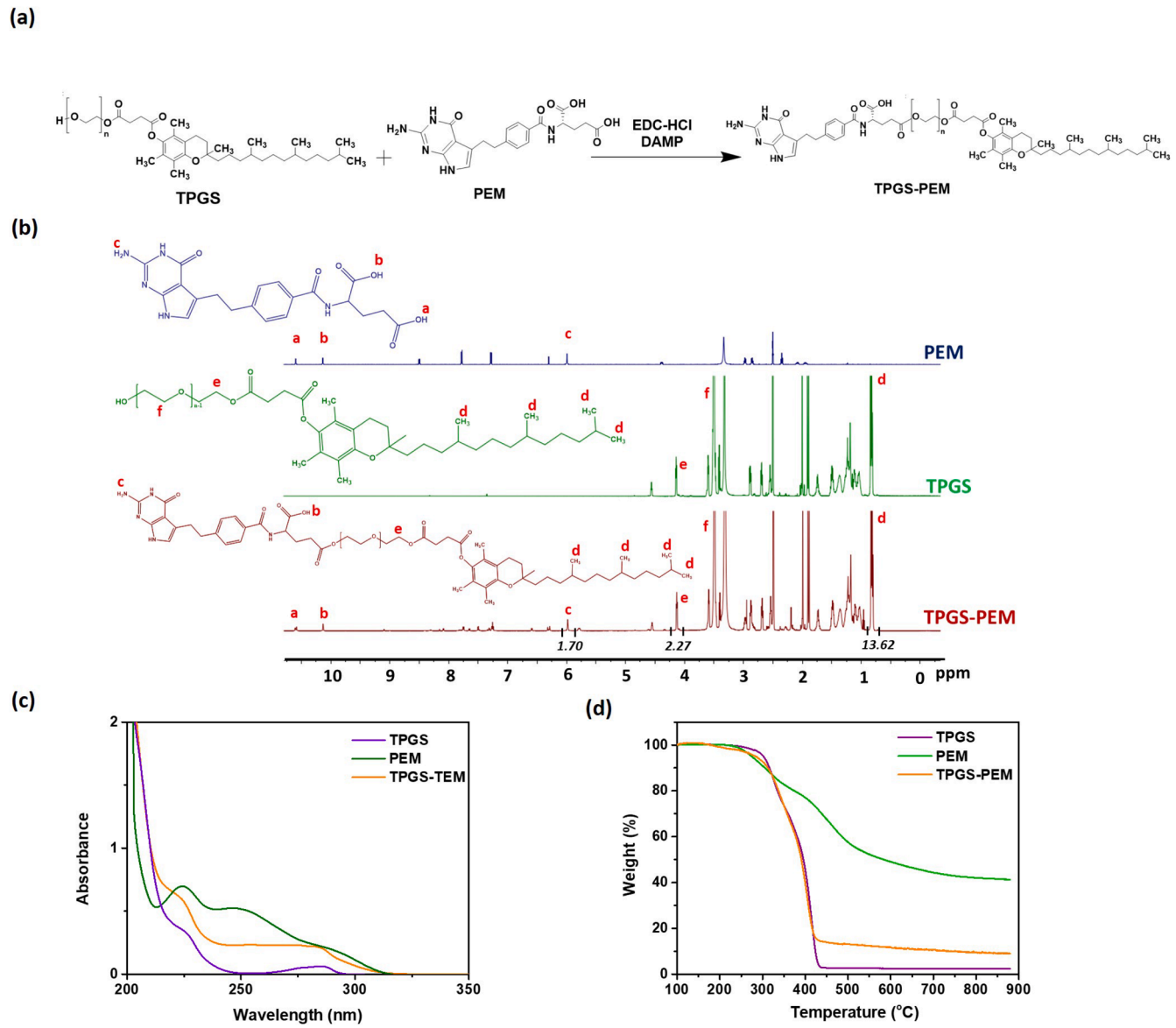

Fig. 1. (a) Synthetic route of TPGS-PEM conjugates. (b) ^{1}H NMR spectra of TPGS, PEM, and TPGS-PEM in DMSO-d_6. (c) UV/Vis spectra and (d) TGA profiles of TPGS, PEM, and TPGS-PEM.

3. Results and discussion

3.1. Synthesis and characterization of TPGS-PEM conjugates

Through the esterification reaction between TPGS and PEM (Fig. 1a), the TPGS-PEM conjugates employed in this work were synthesized and characterized by ^{1}H NMR, UV/Vis spectroscopy, and TGA measurements. As presented in Fig. 1b, the ^{1}H NMR spectrum of TPGS-PEM conjugates displayed the representative proton signals of TPGS at δ 0.81, 3.5, and 4.1 ppm, respectively, and of PEM at δ 6.0, 10.6 and 10.2 ppm, respectively. Also, the characteristic absorption of TPGS at 225 nm and the enhanced absorption from 250 to 275 nm ascribed to PEM were observed in the UV/Vis spectrum of TPGS-PEM adducts (Fig. 1c). These findings verify the coupling of TPGS and PEM to form TPGS-PEM. According to the ^{1}H NMR spectrum, the conjugation efficacy of TPGS with PEM was estimated to be ca 74.9 % by the integral ratio of the methylene proton signals (e, 2H) from TPGS at δ 4.1 ppm to the amine proton signals (c, 2H) from PEM at δ 6.0 ppm. Furthermore, based on the TGA curves of TPGS, PEM, and TPGS-PEM (Fig. 1d) and the detailed calculation presented in the Supporting Information, the TPGS-PEM comprises 82.99 wt % TPGS and 17.01 wt % PEM.

3.2. Preparation and characterization of TDTNs and TDTPNs

To enhance the hydrophobicity of DOX for better encapsulation, the primary amine-containing DOX molecules were complexed with the TA, a natural polyphenol with numerous negatively charged phenolic hydroxyl groups, via the π-π stacking and electrostatic interactions (Scheme 1a). Afterward, through the hydrophobic anchoring and π-π stacking between vitamin E parts from TPGS and TA/DOX complexes, the amphiphilic TPGS segments were further covered on the surfaces of TA/DOX complexes to obtain TDTNs. Without TPGS, the TA/DOX complexes were inclined to aggregate into visible precipitates (Fig. S1a), and inter-particle aggregation was also observed in the TEM images (Fig. S1b). As shown in Table 1 and Fig. 2a, the particle size of TDTNs highly depends on the feeding weight ratio of TA/DOX complexes and TPGS segments. When the weight ratio of TA/DOX complexes and TPGS was fixed at 1:0.6, the attained TDTNs exhibited a large particle size (over 2000 nm). Once the weight ratio was changed from 1:0.6 to 1:1 or 1:1.4, the particle size of TDTNs was remarkably reduced from beyond

Table 1
Particle size, size distribution, and DOX loading characterization of TDTNs with different TA/DOX and TPGS feeding weight ratios.

TA/DOX: TPGS (w/w in feed)	D_h (nm)	PDI	LE (%)
1:0.6	> 2000	-	-
1:1	206.3 ± 7.8	0.270 ± 0.039	96.4 ± 4.8
1:1.4	183.8 ± 18.0	0.215 ± 0.039	36.5 ± 4.8

2000 nm to 206.3 and 183.8 nm (Table 1). These results suggest that the hydrophilic PEG segments of amphiphilic TPGS play a key role in stabilizing the TA/DOX complexes. An adequate amount of TPGS on the surfaces of TA/DOX complexes can avoid aggregation of TDTNs. Moreover, the DOX loading efficiency of TDTNs with a weight ratio of 1:1 was determined to be 96.4 %, being appreciably higher than that (36.5 %) of TDTNs with a weight ratio of 1:1.4. This could be attributed to that excess amphiphilic TPGS segments could decline the interaction between the TA and DOX, thus reducing the encapsulation of DOX into the TDTNs. Notably, in the absence of TA, the DOX and TPGS tended to co-assemble into quite large particles (size beyond 1300 nm), and the DOX loading efficiency was determined to be 28.6 %, appreciably lower than that (96.4 %) of TDTNs. Obviously, the DOX/TPGS assemblies generated from the weak hydrophobic interaction between DOX and TPGS had a loose colloidal structure, thus leading to a remarkable DOX leakage during the dialysis-based purification process. The findings further prove that the formation of TA/DOX dense complexes upon the π-π stacking and electrostatic interactions could enhance DOX hydrophobicity, thus facilitating the incorporation of DOX with TPGS and preventing DOX outflow during purification. Based on the above findings, the TDTPNs were prepared at a fixed weight ratio of 1:1 for TA/DOX and TPGS-PEM to maximize the DOX loading level. It is worth mentioning that the DOX loading content of TDTPNs was determined to be ca 15.4 wt %, which is higher compared to that of the previously reported DOX-loaded nanoparticles, such as amphipathic starch-based nanoparticles (1.3 wt %) [3], U11 peptide-conjugated pH-sensitive DOX/curcumin nanoparticles (8.2 wt %) [1] and onion-like DOX-carrying polymeric nanomicelles (7.1 wt %) [13]. As presented in Fig. 2b and Table 2, the TDTPNs exhibited a smaller particle size (ca 171.7 nm)

Table 2
DLS data and DOX loading characterization of TDTNs and TDTPNs.

Sample	D_h (nm)	PDI	LE (%)	LC (wt %)
TDTNs	206.3 ± 7.8	0.270 ± 0.039	96.4 ± 4.8	12.5 ± 0.6
TDTPNs	171.7 ± 9.2	0.255 ± 0.037	93.0 ± 5.7	15.4 ± 0.7

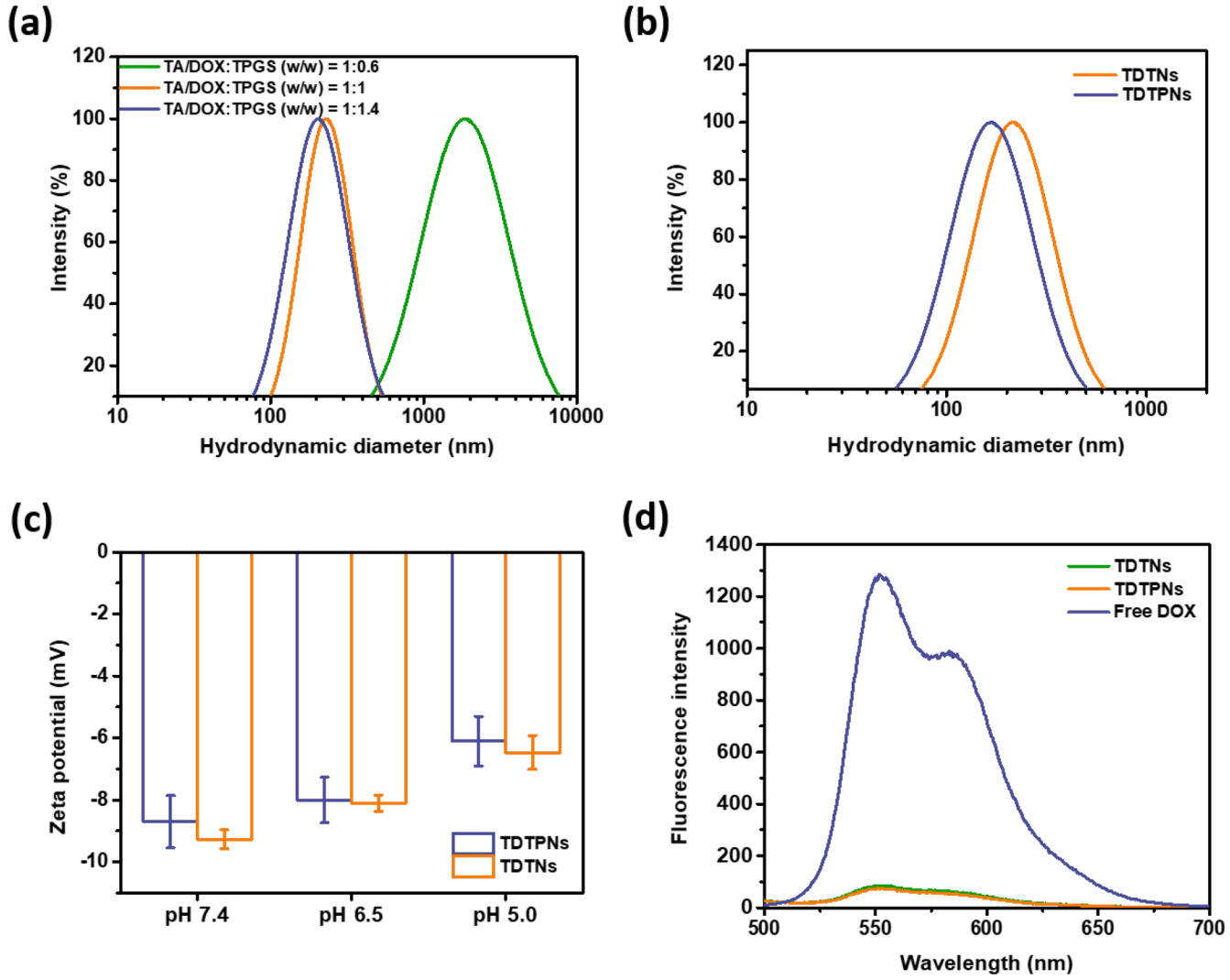

Fig. 2. (a) Particle size distribution profiles of TDTNs with different TA/DOX and TPGS feeding weight ratios. (b) Particle size distribution profiles of TDTNs and TDTPNs dispersed in pH 7.4 PBS. (c) Zeta potential values of TDTNs and TDTPNs dispersed in aqueous solutions with different pH levels. (d) Fluorescence spectra of free DOX molecules, TDTN, and TDTPNs in deionized water (DOX concentration = 3 μM).

than the TDTNs (206.3 nm) and a similar DOX loading capability to TDTNs. Moreover, the zeta potential of TDTPNs dispersed in aqueous solution of pH 7.4 was obtained to be around −8.9 mV, comparable to that of TDTNs (Fig. 2c). Notably, at a fixed DOX concentration of 3 μM, the DOX fluorescence intensity of TDTPNs and TDTNs was profoundly lower relative to that of free DOX (Fig. 2d). This could be ascribed to the massive DOX molecules laden in nano-assemblies, which provoked significant fluorescence self-quenching of DOX, as reported elsewhere [13,31].

Next, the DLS/SLS measurement and TEM were used to explore the morphology of TDTPNs and TDTNs. As shown in Fig. 3a, TDTPNs showed a significant linear relationship between the Γ and q^2, indicating their spherical form [32,33]. Furthermore, the R_g/R_h ratio of TDTPNs was calculated to be ca 0.77, being close to that (0.774) of hard-sphere particles from the self-assembly of diblock copolymer poly [(*N, N*-diethylaminoethyl methacrylate)-*b*-(*N*-isopropyl acrylamide)]s at 25 °C and pH 9.0 as reported by McCormick's group [33]. Also, the TEM images of TDTPNs further illustrate their uniform spherical shape (Fig. 3b). Based on the above findings and the hydrophobic nature of TA/DOX complexes as well as the amphiphilic property of TPGS-PEM conjugates composed of hydrophobic vitamin E and hydrophilic PEM-modified PEG, the TDTPNs were characterized as having a solid spherical form comprising a TA/DOX/vitamin E complex core stabilized by PEM-decorated PEG segments (Scheme 1a). For TDTNs, similar results from DLS/SLS and TEM measurements were also attained (Fig. 3c and d). Furthermore, owing to the transition of TDTPNs and TDTNs from swollen state (DLS) to dried state (TEM), the particle sizes of these nano-assemblies examined by DLS are appreciably larger than those observed by TEM [34].

Considering the structural stability of TDTPNs, a crucial prerequisite for practical anticancer applications, their colloidal stability in pH 7.4 PBS or 10 % fetal bovine serum (FBS)-containing DMEM was assessed by monitoring the particle size over time. As presented in Fig. 4a and b, no significant change in the particle size of TDTPNs dispersed in PBS or FBS-containing DMEM for 24 h was observed. This suggests that the PEG-rich and slightly negatively-charged surfaces of TDTPNs could decrease the absorption of serum protein, thus avoiding inter-particle aggregation. Moreover, the robust hydrophobic and π-π interactions between TA/DOX-constituted complexes and TPGS-PEM segments endow the structural integrity of TDTPNs to prevent the dissociation of nano-assemblies. Notably, the particle size of TDTPNs was gradually enlarged over time in response to a pH change from 7.4 to 5.0 (Fig. 4c). Also, the same pH stimulation elicited a change in the zeta potential of TDTPNs from −8.8 to −6.2 mV (Fig. 2c). These findings suggest that the acidity-induced decreased dissociation degree of TA and the increased protonation of DOX decline electrostatic and π-π stacking interaction of TA with DOX, thereby promoting the structural swelling of TDTPNs. The drug release performance of the TDTPNs and TDTNs was studied at pH 7.4 PBS, mimicking the blood circulation, and at pH 5.0 acetate-buffered saline, imitating the acidic endosomes/lysosomes [35]. As presented in

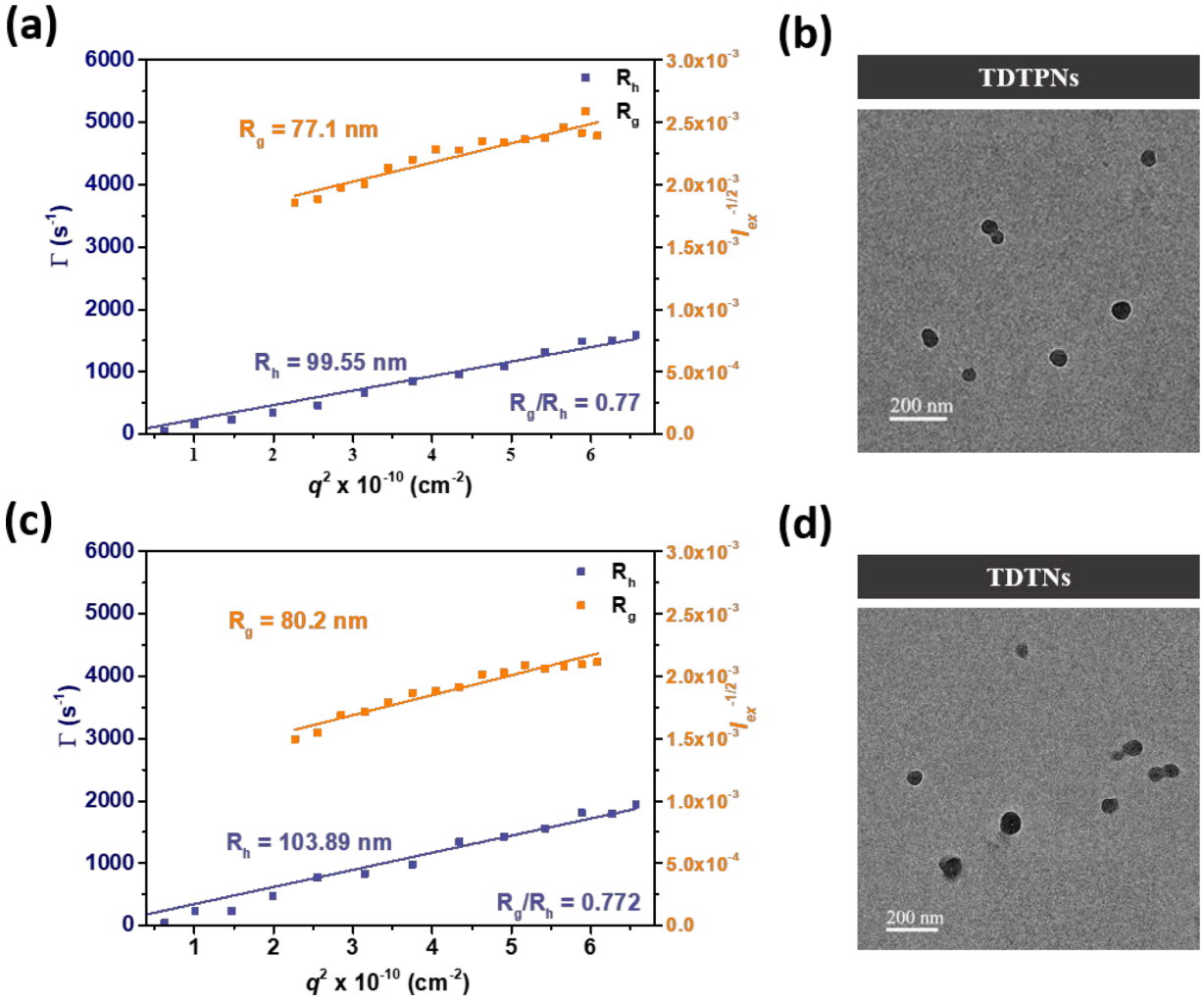

Fig. 3. Correlation function of R_h and Berry plot for R_g of (a) TDTPNs and (c) TDTNs in pH 7.4 PBS attained by DLS/SLS measurement. TEM images of (b) TDTPNs and (d) TDTNs. Scale bars are 200 nm.

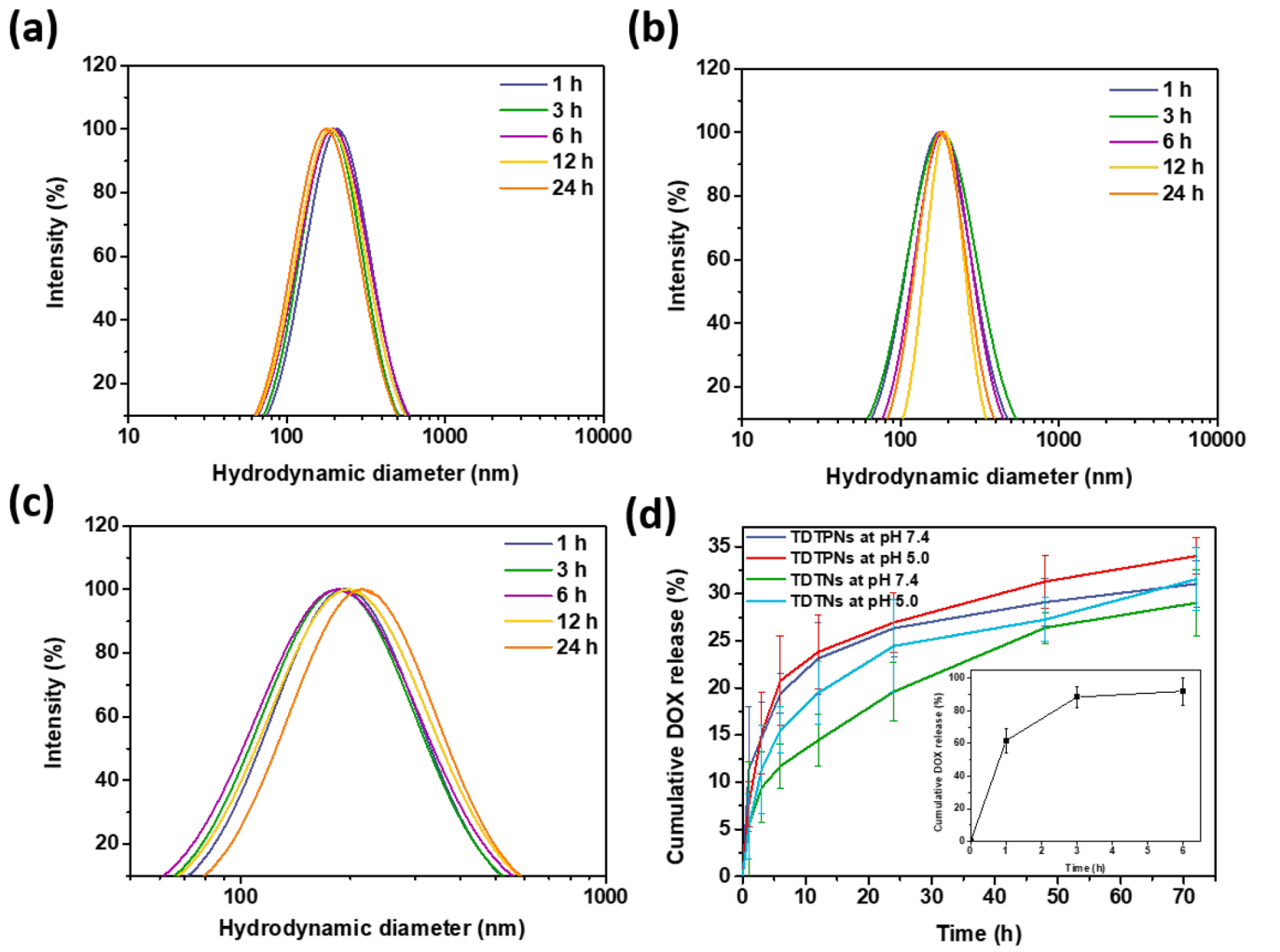

Fig. 4. Particle distribution profiles of TDTPNs dispersed in (a) pH 7.4 PBS, (b) 10 % FBS-containing DMEM, and (c) pH 5.0 acetate buffer at 37 °C. (d) Cumulative DOX liberation behavior of TDTPNs and TDTNs in aqueous pH 7.4 and 5.0 solutions at 37 °C. Inset: passive diffusion of free DOX molecules across the dialysis tube at pH 7.4.

the inset of Fig. 4d, free DOX molecules in the dialysis bag showed rapid outflow in pH 7.4 PBS (beyond 90 % within 6 h). By contrast, in the same environment, a significant decrease in cumulative DOX release (<20 %) from TDTPNs and TDTNs was attained within 12 h (Fig. 4d). This indicates that the strong electrostatic and π-π interactions between TA/DOX complexes within TDTPNs and TDTNs could sufficiently retard the leakage of DOX molecules. Notably, when the solution pH was adjusted from 7.4 to 5.0, the 72 h cumulative releases of DOX from the TDTPNs and TDTNs at pH 5.0 were only marginally higher than that at pH 7.4. This signifies that the acidity-triggered swelling of TDTPNs only slightly increases DOX outflow. However, this would not impact the practical clinical use of the TDTPNs because TPGS, as a biodegradable amphiphilic polymer, could be degraded within cancer cells [36], permitting DOX liberation. Furthermore, the similar DOX release performance of TDTPNs and TDTNs suggests that the PEM surface decoration does not affect the outflow of DOX payloads from the nano-assemblies.

3.3. Cellular uptake study

Some studies reported that the PEM-decorated therapeutic nanoparticles could efficiently target folate receptor-overexpressed cancer cells [27,29,30], enhancing intracellular drug transportation. To explore the folate receptor-targeting performance of TDTPNs, the folate receptor-overexpressed LL/2 Lewis lung carcinoma cells were utilized in the cellular uptake study [37]. As shown in the CLSM images (Fig. 5a), with the incubation time being prolonged from 1 to 4 h, LL/2 cells exposed to TDTPNs exhibited remarkably boosted DOX fluorescence signals compared to free folate-pretreated LL/2 cells incubated with the counterparts. The findings suggest that the TDTPNs could be effectively internalized by LL/2 cells upon folate receptor-mediated endocytosis. In contrast, due to the competition of TDTPNs with free folate molecules for folate receptors of LL/2 cells, their cellular uptake by folate-pretreated LL/2 cells was hindered. Furthermore, to avoid the effects of fluorescence self-quenching of DOX encapsulated within TDTPNs or TDTNs on the observation of cellular uptake, LL/2 cells treated with different formulations were collected and lysed, followed by the addition of DMSO to dissolve internalized nano-assemblies for DOX release and fluorescence measurement. The data on DOX fluorescence intensity showed that the TDTPN group exhibited somewhat higher DOX fluorescence signals than the TDTN group (Fig. 5b and c). This signifies again that the PEM-containing surfaces of TDTPNs could assist their cellular uptake by LL/2 cells via folate receptor-mediated endocytosis (Scheme 1b). Similar observations of the increased cellular internalization of PEM-modified nanoparticles by cancer cells with high expression of folate receptors via folate receptor-mediated endocytosis were also reported by Liu's and Hou's groups [29,30]. Notably, with 1 h and 4 h incubation, the free DOX-treated LL/2 cells displayed remarkably higher DOX fluorescence signals compared to LL/2 cells receiving TDTPNs or TDTNs (Fig. 5). This is because free DOX

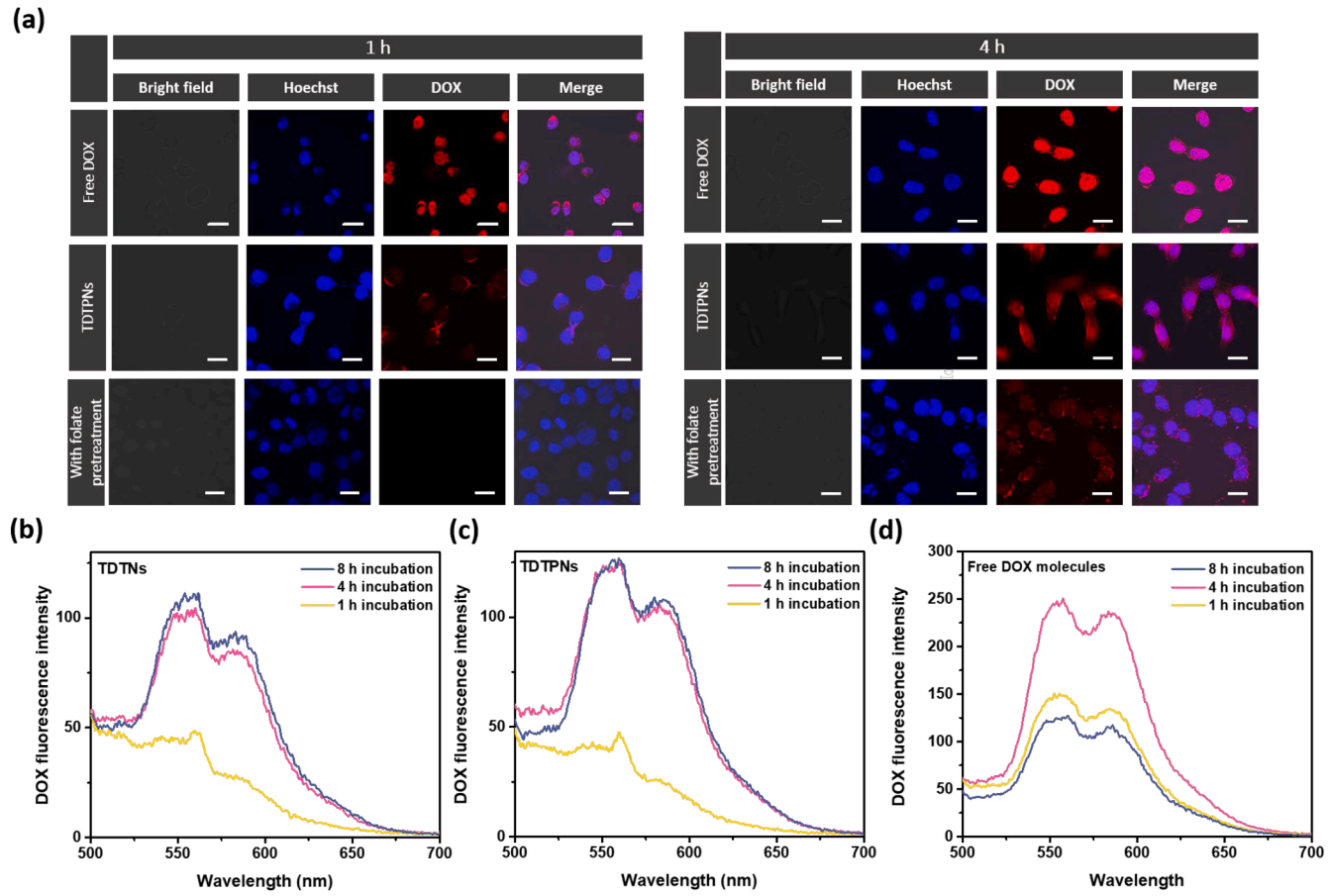

Fig. 5. (a) CLSM images of LL/2 cells exposed to free DOX molecules, TDTPNs, or TDTPNs with the addition of free folate at 37 °C for 1 and 4 h. Scale bars are 20 μm. Fluorescence spectra of DOX molecules from LL/2 cells incubated with (b) TDTNs, (c) TDTPNs, and (d) free DOX molecules, respectively, for 1, 4, and 8 h.

molecules quickly penetrate through the cell membrane into cancer cells by passive diffusion while DOX-carrying nanoparticles are internalized by cancer cells via slow endocytosis [38,39]. Interestingly, when the incubation time was further prolonged from 4 to 8 h, it was found that the fluorescence intensity of DOX from LL/2 cells incubated with free DOX molecules significantly declined (Fig. 5d). In contrast, the DOX fluorescence intensity from the LL/2 cells receiving TDTPNs or TDTNs remained nearly unchanged. This may be because of the following reasons. First, the P-gp on cell membranes of LL/2 cells could promote ATP-driven DOX efflux from their cytoplasm, thus leading to the resistance of LL/2 cells to free DOX molecules. Because the non-ionic TPGS has been demonstrated to diminish drug resistance of cancer cells by disturbing and disrupting membrane structure [23–25], it is reasonably assumed that the TPGS-containing TDTPNs and TDTNs probably enhance intracellular DOX accumulation by inhibiting the activity of P-gp on cell membranes. Li et al. also reported that the TPGS-coated and DOX-loaded cationic liposomes effectively enhanced the accumulation of DOX molecules within drug-resistant Human hepatocellular carcinoma Bel7402 cells by inhibiting the P-gp efflux pump [40].

3.4. *In vitro cytotoxicity study*

To evaluate the anticancer effect of TDTPNs, their in vitro cytotoxicity against LL/2 cells was assessed by the MTT method. As shown in Fig. 6a, as an important control, LL/2 cells incubated with TA (0.09~1.4 μM) or TPGS (0.16~2.61 μM) for 24 h showed high viability (beyond 95 %), suggesting that these materials, as crucial components of TDTPNs and TDTNs, were nearly harmless to LL/2 cells. When LL/2 cells were incubated with free DOX molecules, TDTPNs, or TDTNs in the DOX concentration range 0.16~2.5 μM, the cell viability appreciably declined with increased drug concentration (Fig. 6b), suggesting the topoisomerase II inhibition of DOX to cause DNA double-strand breaks and cytotoxicity. Notably, for TDTPNs and TDTNs, the half maximal inhibitory concentration (IC50) of DOX for cancer cell viability was estimated to be ca 0.277 and 0.361 μM (Fig. 6c), being somewhat lower than that (0.542 μM) of free DOX molecules, indicating that the TDTPNs and TDTNs exhibited anticancer effect higher to free DOX molecules. Obviously, the promoted intracellular DOX delivery of TDTPNs and TDTNs upon TPGS-mediated inhibition in P-gp activation of LL/2 cells enhanced their cytotoxicity. Notably, compared to TDTNs, the TDTPNs displayed a few higher cytotoxicity against LL/2 cells. For other human NSCLC PC9 cells with overexpressed folate receptors [41], the TDTPNs also displayed anticancer activity superior to TDTNs (Fig. 6d). Furthermore, it should be mentioned that the viability of LL/2 cells and PC9 cells treated with PEM molecules declined moderately with increasing PEM concentration due to the anticancer activity of PEM by interfering with several enzymes of the folate pathway [26,27]. On the other hand, the TDTPNs showed low cytotoxicity on the healthy WS1 cells, human skin fibroblast cells, as revealed in Fig. S2, being attributed to their poor cellular uptake by WS1 cells with low expression of folate receptors. According to the above findings, the PEM-decorated TDTPNs could increase intracellular DOX and PEM delivery by folate receptor-mediated endocytosis to boost the anticancer potency against NSCLC and decrease undesired cytotoxicity on normal cells. Therefore, through the EPR effect and PEM-mediated tumor targeting, the TDTPNs were anticipated to be accumulated within tumor sites to boost anticancer efficacy and reduce adverse effects. In the future, to prove the feasibility of TDTPNs in the NSCLC treatment, some research works, including in vivo biodistribution and antitumor growth inhibition, will be conducted and discussed.

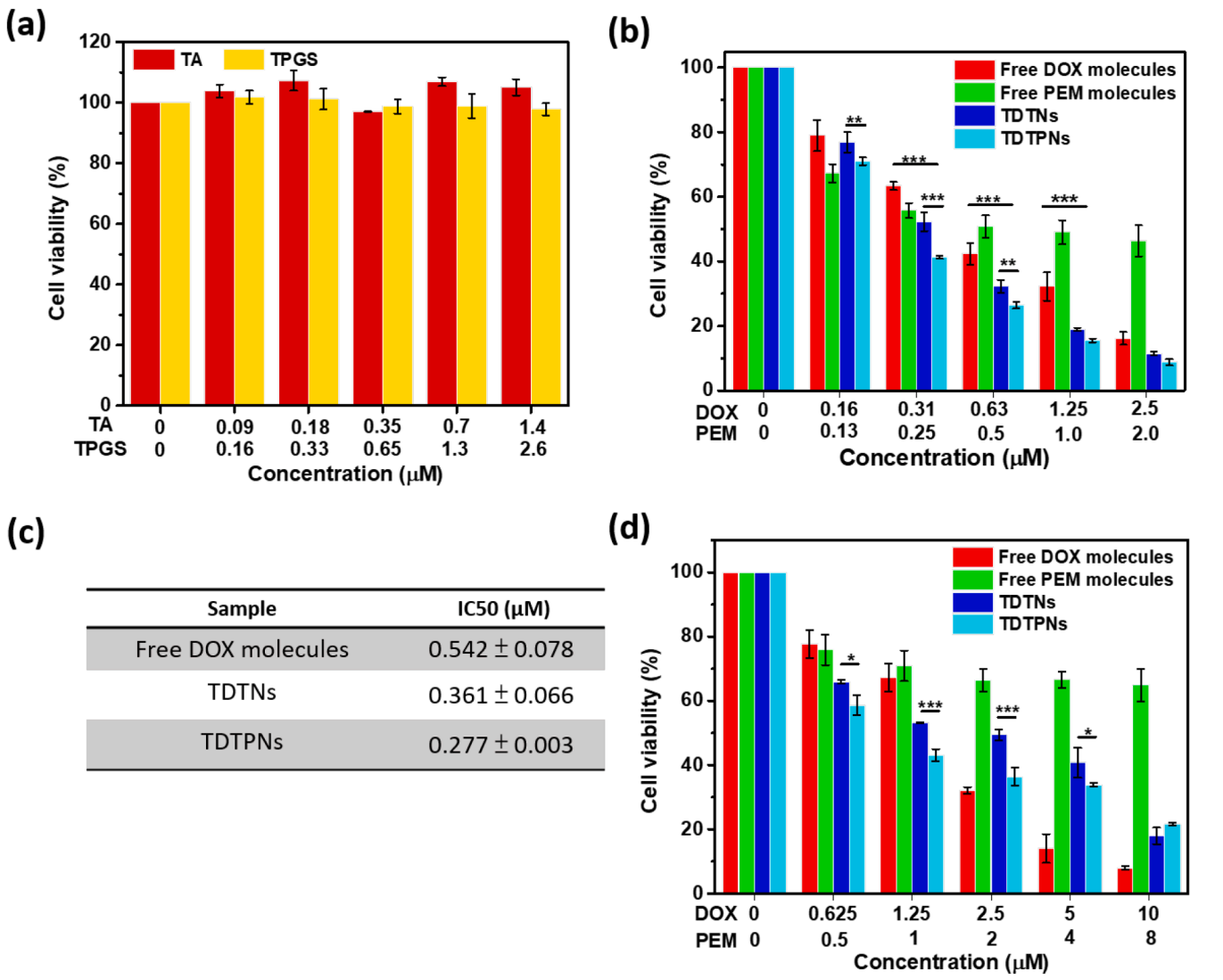

(c)

Sample	IC50 (μM)
Free DOX molecules	0.542 ± 0.078
TDTNs	0.361 ± 0.066
TDTPNs	0.277 ± 0.003

Fig. 6. (a) Cell viability of LL/2 cells treated with TA or TPGS of different concentrations at 37 °C for 24 h. (b) Cell viability of LL/2 cells receiving free DOX molecules, free PEM molecules, TDTNs, and TDTPNs, respectively, at 37 °C for 24 h. (c) IC50 values of free DOX molecules, TDTNs, and TDTPNs on LL/2 cells. (d) Cell viability of PC9 cells incubated with free DOX molecules, free PEM molecules, TDTNs, and TDTPNs, respectively, at 37 °C for 48 h.

4. Conclusions

In this work, we successfully created the folate receptor-targeting and DOX-carrying nano-assemblies using a one-step and organic solvent-free method for improved NSCLC treatment. The as-synthesized TPGS-PEM conjugates were attached to TA/DOX assemblies through hydrophobic and π-π stacking interactions to attain the TDTPNs with folate receptor-targeting capability. The angle-dependent DLS/SLS results and TEM images indicate that the TDTPNs have a well-dispersed spherical shape. Taking advantage of the π-π stacking and electrostatic attractions between TA and DOX, the TDTPNs showed prominent drug loading capacity (ca 15.4 wt %) and effectively reduced premature DOX leakage in pH 7.4 PBS. Moreover, the TDTPNs displayed outstanding colloidal stability in serum-rich DMEM. Compared to TDTNs, the TDTPNs were efficiently internalized by LL/2 cells through folate receptor-mediated endocytosis. Moreover, the TDTPNs and TDTNs progressively promoted DOX accumulation within LL/2 cells upon TPGS-mediated P-gp inactivation. Compared to TDTNs, the TDTPNs showed a superior anticancer effect on the LL/2 and PC9 cells, suggesting great potential for treating NSCLC.

CRediT authorship contribution statement

Wei-Jen Huang: Methodology, Investigation, Formal analysis, Conceptualization. **Wen-Hsuan Chiang:** Writing – original draft, Supervision, Resources, Investigation, Funding acquisition. **Hsiang-Yun Chih:** Validation, Methodology. **I-Ju Liu:** Methodology, Investigation. **Jeng-Sen Tseng:** Writing – review & editing, Supervision, Project administration, Funding acquisition, Conceptualization. **Tsung-Ying Yang:** Resources, Investigation, Funding acquisition.

Declaration of competing interest

The authors declare that they have no known competing financial interests or personal relationships that could have appeared to influence the work reported in this paper.

Acknowledgments

This work is supported by the National Science and Technology Council (NSTC 113–2221-E-005–010-MY2 and NSTC 113–2628-E-005–002-MY3), National Chung Hsing University and Taichung Veterans General Hospital (TCVGH—NCHU 1137602), Taiwan.

Supplementary materials

Supplementary material associated with this article can be found, in the online version, at doi:10.1016/j.jtice.2025.106115.

References

[1] Hong Y, Che S, Hui B, Yang Y, Wang X, Zhang X, Qiang Y, Ma H. Lung cancer therapy using doxorubicin and curcumin combination: targeted prodrug based, pH sensitive nanomedicine. Biomed Pharmacother 2019;112:108614.

[2] Moradi A, Shirangi A, Asadi M, Farokhi M, Gholami M, Aminianfarf H, Atyabi F, Mottaghitalab F, Dinarvand R. Targeted delivery of doxorubicin by SP5-52 peptide conjugated exosome nanoparticles into lung tumor: an in vitro and in vivo study. J Drug Deliv Sci Technol 2024;92:105313.

[3] Li K, Zhan W, Jia M, Zhao Y, Liu Y, Jha RK, Zhou L. Dual loading of nanoparticles with doxorubicin and icotinib for the synergistic suppression of non-small cell lung cancer. Int J Med Sci 2020;17:390–402.

[4] Melguizo C, Cabeza L, Prados J, Ortiz R, Caba O, Rama AR, Delgado AV, Arias JL. Enhanced antitumoral activity of doxorubicin against lung cancer cells using biodegradable poly(butylcyanoacrylate) nanoparticles. Drug Des Devel Ther 2015;9:6433–44.

[5] Ahmad A, Gadgeel SM. Lung cancer and personalized medicine: novel therapies and clinical management preface. Adv Exp Med Biol 2016;890.

[6] Kocher F, Hilbe W, Seeber A, Pircher A, Schmid T, Greil R, Auberger J, Nevinny-Stickel M, Sterlacci W, Tzankov A, Jamnig H, Kohler K, Zabernigg A, Frötscher J, Oberaigner W, Fiegl M. Longitudinal analysis of 2293 NSCLC patients: a comprehensive study from the TYROL registry. Lung Cancer 2015;87:193–200.

[7] Yano T, Okamoto T, Fukuyama S, Maehara Y. Therapeutic strategy for postoperative recurrence in patients with non-small cell lung cancer. World J Clin Oncol 2014;5:1048–54.

[8] Schiller JH, Harrington D, Belani CP, Langer C, Sandler A, Krook J, Zhu J, Johnson DH. Eastern cooperative oncology group, comparison of four chemotherapy regimens for advanced non-small-cell lung cancer. N Engl J Med 2002;346:92–8.

[9] Grossi F, Gridelli C, Aita M, De Marinis F. Identifying an optimum treatment strategy for patients with advanced non-small cell lung cancer. Crit Rev Oncol Hematol 2008;67:16–26.

[10] Mdlovu NB, Lin KS, Weng MT, Mdlovu NV. Formulation and in-vitro evaluations of doxorubicin loaded polymerized magnetic nanocarriers for liver cancer cells. J Taiwan Inst Chem Eng 2021;126:278–87.

[11] Mdlovu NV, Lin KS, Mavuso FA, Weng MT. Preparation, characterization, and in-vitro studies of doxorubicin-encapsulated silica coated iron oxide nanocomposites on liver cancer cells. J Taiwan Inst Chem Eng 2020;117:190–7.

[12] Duan X, Wang Q, Che W, Li T, Zhang K, Han L, Song L, Guo W. Redox-responsive nanomedicine of doxorubicin-conjugated poly-L-glutathione oxidized for cancer therapy. J Taiwan Inst Chem Eng 2024;159:105456.

[13] Huang SY, Yeh NT, Wang TH, Hsu TC, Chin HY, Tzang BS, Chiang WH. Onion-like doxorubicin-carrying polymeric nanomicelles with tumor acidity-sensitive dePEGylation to expose positively-charged chitosan shell for enhanced cancer chemotherapy. Int J Biol Macromol 2023;227:925–37.

[14] Pawar CS, Rajendra Prasad N, Yadav P, Muthu Vijayan Enoch IV, Manikantan V, Dey B, Baruah P. Enhanced delivery of quercetin and doxorubicin using β-cyclodextrin polymer to overcome P-glycoprotein mediated multidrug resistance. Int J Pharm 2023;635:122763.

[15] Cheng W, Liang C, Xu L, Liu G, Gao N, Tao W, Luo L, Zuo Y, Wang X, Zhang X, Zeng X, Mei L. TPGS-functionalized polydopamine-modified mesoporous silica as drug nanocarriers for enhanced lung cancer chemotherapy against multidrug resistance. Small 2017;13:1700623.

[16] Shen MY, Chen YH, Yeh NT, Wang TH, Chiang WH. Acidity/hydrogen peroxide-responsive PEGylated chitosan-modified polydopamine nanoparticles to realize effective photothermal conversion and intracellular drug delivery. Eur Polym J 2023;197:112365.

[17] Xue K, Wei F, Lin J, Tian H, Zhu F, Li Y, Hou Z. Tumor acidity-responsive carrier-free nanodrugs based on targeting activation via ICG-templated assembly for NIR-II imaging-guided photothermal-chemotherapy. Biomater Sci 2021;9:1008–19.

[18] Liang KA, Chih HY, Liu IJ, Yeh NT, Hsu TC, Chin HY, Tzang BS, Chiang WH. Tumor-targeted delivery of hyaluronic acid/polydopamine-coated Fe^{2+}-doped nano-scaled metal-organic frameworks with doxorubicin payload for glutathione depletion-amplified chemodynamic-chemo cancer therapy. J Colloid Interface Sci 2025;677:400–15.

[19] Aziz A, Sefidbakht Y, Rezaei S, Kouchakzadeh H, Uskoković V. Doxorubicin-loaded, pH-sensitive albumin nanoparticles for lung cancer cell targeting. J Pharm Sci 2022;111:1187–96.

[20] Moles E, Chang DW, Mansfeld FM, Duly A, Kimpton K, Logan A, Howard CB, Thurecht KJ, Kavallaris M. EGFR targeting of liposomal doxorubicin improves recognition and suppression of non-small cell lung cancer. Int J Nanomedicine 2024;19:3623–39.

[21] Kaur P, Garg T, Rath G, Murthy RS, Goyal AK. Surfactant-based drug delivery systems for treating drug-resistant lung cancer. Drug Deliv 2016;23:727–38.

[22] Yuan X, Ji W, Chen S, Bao Y, Tan S, Lu S, Wu K, Chu Q. A novel paclitaxel-loaded poly(d,l-lactide-co-glycolide)-tween 80 copolymer nanoparticle overcoming multidrug resistance for lung cancer treatment. Int J Nanomedicine 2016;11:2119–31.

[23] Luiz MT, Filippo LDD, Alves RC, Araújo VHS, Duarte JL, Marchetti JM, Chorilli M. The use of TPGS in drug delivery systems to overcome biological barriers. Eur Polym J 2021;142:110129.

[24] Yang C, Wu T, Qi Y, Zhang Z. Recent advances in the application of vitamin E TPGS for drug delivery. Theranostics 2018;8:464–85.

[25] Wang X, Xu X, Zhang S, Chen N, Sun Y, Ma K, Hong D, Li L, Du Y, Lu X, Jiang S. TPGS-based and S-thanatin functionalized nanorods for overcoming drug resistance in Klebsiella pneumonia. Nat Commun 2022;13:3731.

[26] Kwok WC, Cheong TF, Chiang KY, Ho JCM, Lam DCL, Ip MSM, Tam TCC. Haematological toxicity of pemetrexed in patients with metastatic non-squamous non-small cell carcinoma of lung with third-space fluid. Lung Cancer 2021;152:15–20.

[27] Rosch JG, DuRoss AN, Landry MR, Sun C. Development of a pemetrexed/folic acid nanoformulation: synthesis, characterization, and efficacy in a murine colorectal cancer model. ACS Omega 2020;5:15424–32.

[28] Hanauske AR, Chen V, Paoletti P, Niyikiza C. Pemetrexed disodium: a novel antifolate clinically active against multiple solid tumors. Oncologist 2001;6:363–73.

[29] Li Y, Lin J, Wang P, Luo Q, Lin H, Zhang Y, Hou Z, Liu J, Liu X. Tumor microenvironment responsive shape-reversal self-targeting virus-inspired nanodrug for imaging-guided near-infrared-II photothermal chemotherapy. ACS Nano 2019;13:12912–28.

[30] Yang Y, Fan Z, Zheng K, Shi D, Su G, Ge D, Zhao Q, Fu X, Hou Z. A novel self-targeting theranostic nanoplatform for photoacoustic imaging-monitored and enhanced chemo-sonodynamic therapy. J Mater Chem B 2021;9:5547–59.

[31] Wang W, Sun H, Meng F, Ma S, Liu H, Zhong Z. Precise control of intracellular drug release and anti-tumor activity of biodegradable micellar drugsvia reduction-sensitive shell-shedding. Soft Matter 2012;8:3949–56.

[32] Kogej K, Božič D, Kobal B, Herzog M, Černe K. Application of dynamic and static light scattering for size and shape characterization of small extracellular nanoparticles in plasma and ascites of ovarian cancer patients. Int J Mol Sci 2021;22:12946.

[33] Smith AE, Xu X, Kirkland-York SE, Savin DA, McCormick CL. Schizophrenic" self-assembly of block copolymers synthesized via aqueous RAFT polymerization: from micelles to vesicles. Macromolecules 2010;43:1210–7.

[34] Hung YN, Liu YL, Chou YH, Hu SH, Cheng B, Chiang WH. Promoted cellular uptake and intracellular cargo release of ICG/DOX-carrying hybrid polymeric nanoassemblies upon acidity-activated PEG detachment to enhance cancer photothermal/chemo combination therapy. Euro Polym J 2022;163:110944.

[35] Kievit FM, Wang FY, Fang C, Mok H, Wang K, Silber JR, Ellenbogen RG, Zhang M. Doxorubicin loaded iron oxide nanoparticles overcome multidrug resistance in cancer in vitro. J Control Release 2011;152:76–83.

[36] Ren T, Li R, Zhao L, Fawcett JP, Sun D, Gu J. Biological fate and interaction with cytochromes P450 of the nanocarrier material, D-a-tocopheryl polyethylene glycol 1000 succinate. Acta Pharm Sin B 2022;12:3156–66.

[37] Tie Y, Zheng H, He Z, Yang J, Shao B, Liu L, Luo M, Yuan X, Liu Y, Zhang X, Li H, Wu M, Wei Z. Targeting folate receptor β positive tumor-associated macrophages in lung cancer with a folate-modified liposomal complex. Signal Transduct Target Ther 2020;5:6.

[38] Zhang Y, Li P, Pan H, Liu L, Ji M, Sheng N, Wang C, Cai L, Ma Y. Retinal-conjugated pH-sensitive micelles induce tumor senescence for boosting breast cancer chemotherapy. Biomaterials 2016;83:219–32.

[39] Chang D, Gao Y, Wang L, Liu G, Chen Y, Wang T, Tao W, Mei L, Huang L, Zeng X. Polydopamine-based surface modification of mesoporous silica nanoparticles as pH-sensitive drug delivery vehicles for cancer therapy. J Colloid Interface Sci 2016;463:279–87.

[40] Li Y, Tan X, Liu X, Liu L, Fang Y, Rao R, Ren Y, Yang X, Liu W. Enhanced anticancer effect of doxorubicin by TPGS-coated liposomes with bcl-2 siRNA-corona for dual suppression of drug resistance. Asian J Pharm Sci 2020;15:646–60.

[41] Xu Y, Jin X, Zhang J, Wang K, Jin X, Xu D, Tian X, Liu L. Antitumor activity of a novel double-targeted system for folate receptor-mediated delivery of mitomycin C. ACS Omega 2020;5:26864–70.